

A Single Time Scale Visual Servoing System for a High Speed SCARA Type Robotic Arm

Migara H. Liyanage and Nicholas Krouglicof

Abstract—A high speed image based visual servoing (VS) technique is developed in this study for a Selective Compliant Assembly Robotic Arm (SCARA) manipulator with rotary hydraulic actuators. This study has developed a 2D position measuring system which comprise a high speed camera with a position sensitive detector as the image sensor. The input output interface and the controller for the VS system was implemented using a field programmable gate array (FPGA) providing a single chip solution for the embedded system. This camera was capable of providing position measurements of the end effector (EE) with an accuracy of up to 0.95 mm at a frequency of 1340 Hz. The proposed control strategy produced a better tracking performance with an EE payload of 12 kg with speeds of up to 1.3 m/s.

I. INTRODUCTION

This paper considers the issue of tracking the end effector position of a high speed robotic manipulator interacting with a large payload. When serial manipulators move at high speeds, the vibration resulting from the compliance of the supporting structure combined with the elastic deformation of the links yields significant discrepancies in the end effector (EE) position with respect to the desired trajectory. This problem can be alleviated by accurately measuring the actual position of the EE with respect to (w.r.t.) an external reference frame and incorporating this information in the robot control strategy. Visual Servoing (VS) refers specifically to the integration of vision based feedback in the robot control loop in order to mitigate the effects of disturbances and achieve increased accuracy. The problem of fine position control of a manipulator is a well-studied research topic but in practice, it is seldom resolved using visual servoing techniques. When commercially available image sensors are used as the exteroceptive sensors in VS, feedback data on the end effector position is generally acquired at a much slower rate than data from the proprioceptive sensors (e.g.; joint encoders). Visual servoing becomes even more challenging when the end effector (EE) moves at extremely high speeds. Researchers have devised a number of strategies to circumvent the bandwidth and computational challenges including a multi sensor two time scale approach [1], [2].

Vision-based feedback was used by Jiang and Eguchi [2] for EE tracking control of a flexible manipulator; however, their robot is much simpler and moves at much slower speeds (on the order of 40 mm/s) compared to the manipulator

employed in this study. Liu et al. [3] proposed a hybrid, multi-sensor approach for accurate, robot target tracking. This method used a CCD camera to implement an image based visual servoing (IBVS) technique for coarse positioning and a PSD for the final accurate positioning of the EE. In another study Bascetta et al. [1] adopted a two time scale visual servoing strategy for flexible manipulators. It uses a fast controller that employs feedback from proprioceptive sensors (strain gauges) which operates at 500 Hz. The visual control law which is executed every 40 ms (25 Hz), ensures smooth tracking of the desired trajectory. Hitaka et. al [4] considered a stereo-vision-based method to estimate the oscillation of a mobile manipulator; however, the stereo vision system considered in this study is not suitable for high speed applications. The control problems associated with visual servoing have been widely studied [5]. Kelly [6], proposed an image-based controller which is Lyapunov stable with the uncertainties in radial lens distortions and camera orientation. In another study Marey and Chaumette [7] proposed a series of image based visual servoing control laws. The proposed control laws were based on achieving global stability of the system. There are also a number of studies that address the object measurement problem [5]; however, these studies did not consider high speed manipulator systems or the development of appropriate hardware for industrial applications.

Image based visual servoing (IBVS) requires the estimation of position and orientation of the EE from one or more cameras. A wide range of commercially available cameras have been employed for IBVS. High resolution cameras based on the Charge Coupled Device (CCD) have been used for various position estimation applications in a number of studies [8], [9]. Complementary Metal Oxide Semiconductor (CMOS) cameras that produce high quality images at much higher speeds have emerged as an alternative to the conventional CCD cameras [10]. In recent years motion capture system have been considered in various robot positioning applications. The ARTTrack2 [11] motion capture system was considered for tracking and control of the EE of a light-weight surgical robot. The Vicon motion capture system [12], [13] has been widely used for tracking and controlling the trajectory of quadrotor UAVs. These systems require more physical space for setup and their use has been limited to applications that require low sampling rates.

The main objective of this study is to develop a single time scale visual servoing system for an extremely high speed industrial manipulator. The ultimate goal is to realize a low cost, single chip controller for robotic applications. The

*This work is supported by the Atlantic Canada Opportunities Agency (ACOA), Research & Development Corporation of Newfoundland & Labrador (RDC).

The authors are with Faculty of Engineering & Applied Science, Memorial University of Newfoundland, St Johns, Newfoundland, Canada, A1B 3X5. mh1545 & nickk@mun.ca

image sensor selected to acquire visual feedback information on the EE must be fast and simple to integrate into the robot controller. Camera systems based on CCD or CMOS technology are expensive and require significant computational resources. In contrast, Position Sensitive Detectors (PSDs) provide a simple, efficient, and cost effective solution for high speed, non-contact position measurement. Furthermore, these sensors require only simple signal conditioning electronics, they can operate at high speeds, and the position estimation is computationally simple. Wang et al. [14] developed a similar camera system using a 2D PSD. However, measurements made using this camera contain a significant amount of noise and had to use multiple sensor fusion for noise elimination. It also did not provide a hardware interface that could be used for real time controls.

The proposed high speed, single time scale VS system integrates both a 2D PSD-based optical position sensing system as the exteroceptive sensor, and high resolution joint encoders as proprioceptive sensors. A single chip solution based on reconfigurable hardware was adopted for implementing the complete controller architecture including the interfaces for the sensor suite as well as the computational elements associated with the kinematics and control laws. For the optical position sensing system, a 2D PSD was integrated with an optical assembly, dedicated signal conditioning and data acquisition electronics, a specially designed active target marker, and a spectrally matched optical interference filter. A rigorous calibration procedure was performed on the optical position sensing system in order to ensure the accuracy of the measurements. The entire robot controller was implemented exclusively in a Cyclone III Field Programmable Gate Array (FPGA). A virtual processor was synthesized and implemented in the same FPGA to handle the computational intensive elements of the controller. The proposed VS system was extensively tested using a high speed hydraulic SCARA manipulator developed at the Memorial University. This manipulator is capable of handling payloads in the range of 10 to 20 kg while operating at speeds of up to 2.1 ms^{-1} [15].

This paper is organized as follows. It starts with an introduction to the study. Section 2 provides the details of the controller of the VS system. Section 3 outlines the development of the high speed camera. Section 4 details the on site calibration algorithm. Section 5 presents the FPGA-based control system architecture. Section 6 presents the experimental setup. The experimental results from this study are presented in Section 7. The conclusions are given in Section 8.

II. CONTROLLER FOR THE VS SYSTEM

The SCARA type robotic arm considered in this study has links of length l_2 and l_3 . The relative joint angles of the links will be given by θ_2 and θ_3 . The proposed VS system will use feedback from optical encoders for joint angle and position of the EE obtained from the high speed camera. A schematic diagram of the proposed system is shown in Fig. 1.

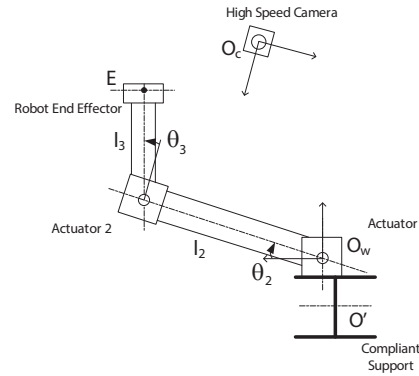


Fig. 1. Plan view of the SCARA arm with the VS system

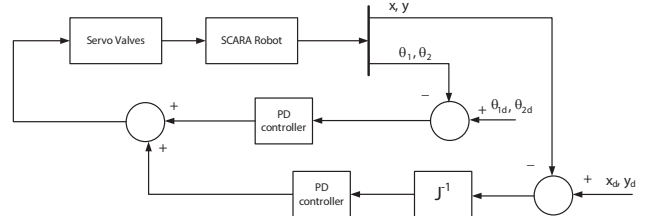


Fig. 2. A schematic diagram showing the architecture of the proposed controller

The feedback for controlling the arm will be obtained using both proprioceptive (encoders) and exteroceptive sensors (high speed camera). The encoder angles will provide the relative position of the links. During the high speed motion of the robot flexing of the links and torsional vibration of the support column could affect the final position of the EE. Therefore, accurate position control of the EE requires to consider the absolute position the EE. A schematic diagram of the proposed controller is shown in Fig. 2.

The control signal (U) for the servo valves will calculated considering joint angles and EE position. This will be given by,

$$U = K_{P\theta}.e_\theta + K_{D\theta}.e'_\theta + K_{PXY}.J^{-1}.e_{XY} + K_{DXY}.(J^{-1}.e'_{XY}) \quad (1)$$

Where, $K_{P\theta}, K_{PXY}$ are a set of proportional gains, $K_{D\theta}, K_{DXY}$ are a set of derivative gains, e_θ is the difference between desired and actual link angles, e_{XY} is the difference between the desired and actual position of the EE in Cartesian coordinates with respect to a world coordinate system and J^{-1} corresponds to the inverse of the manipulator Jacobian.

III. THE DEVELOPMENT OF A HIGH SPEED CAMERA FOR POSITION MEASUREMENT

The high speed imaging device consists of a camera with the Hamamatsu[®] (S5991-01) improved tetra-lateral (pin cushion) type 2D PSD as the image sensor. It comprises one cathode and four anodes. When a light spot is projected on to

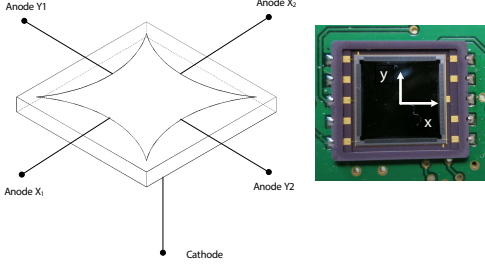


Fig. 3. The Hamamatsu S5991 2D PSD

the image sensor it would result in currents being induced in the anodes due to a phenomena known as the photo electric effect. It has a peak sensitivity to infra red signals. Hence, an infra red (IR) source is used as the beacon. The magnitude of these current signals vary depending on the location of the projected light spot on the image sensor. This PSD has an active area of 9 x 9 mm. A schematic diagram of this PSD is shown in Fig. 3.

When the PSD is illuminated by an IR source the magnitudes of the induced currents depend on the distance between the illuminated point and the four anodes. Hence, the x , y coordinates of the spot of illumination could be calculated using the equation [16],

$$\bar{X} = \frac{(I_2 + I_3) - (I_1 + I_4)}{I_1 + I_2 + I_3 + I_4} \quad (2)$$

$$\bar{Y} = \frac{(I_2 + I_4) - (I_1 + I_3)}{I_1 + I_2 + I_3 + I_4}, \quad (3)$$

Where I_1, I_2, I_3, I_4 correspond to the induced currents in the PSD, and \bar{X} , \bar{Y} are dimensionless relative distances in $-x$, $-y$ directions. These equations give dimensionless quantities for both X and Y . These quantities should be related to a physical position quantity to be used for position measurement applications. Hence, the PSD should be calibrated to estimate the nonlinear relationship between \bar{X} , \bar{Y} and the position of the light spot on the image sensor.

A. Design of the Signal Conditioning Circuit for the Camera

The PSD needs to be reverse biased with the cathode at +10 V and the four anodes at +5V for operation. The biasing voltages should be stable. Hence, it will be generated using a +5V LT1019 precision voltage reference. The voltage that is induced from photo current contains noise and requires signal conditioning. A first order (low pass) filter is used for this. It will attenuate shot noise and pass other signals with frequencies lower than the cutoff frequency. Experiments showed that the filter required an integration time of 84 μ s on each anode. This induced voltage is a very weak electric signal. Therefore, it requires signal amplification to transform the weak current signal to a measurable voltage signal. The OP495 high precision operational amplifier is used for signal conditioning and signal amplification.

The analog currents induced from the IR signal should be converted into digital signals for data acquisition. This could

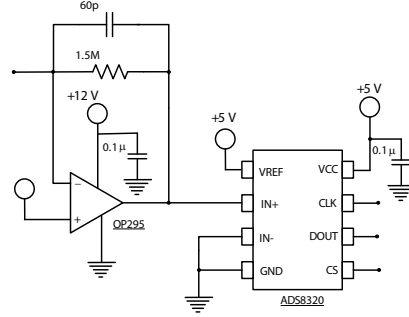


Fig. 4. A schematic diagram of the printed circuit board for PSD signal conditioning and data acquisition

be done with an analog to digital converter (ADC). As this system is used for making high speed measurements the data acquisition system should be fast and accurate. Therefore, a 16-bit ADC (ADS8320) is used for data acquisition. This ADC chip is capable of operating at data rates of up to 100 kHz with a resolution of up to 0.1 mV. The anode voltages are acquired as 16 bit digital signals through a Serial Peripheral Interface (SPI) input type interface. A schematic diagram of the first order low pass filter circuit along with the ADC and the printed circuit board (PCB) developed for image sensor is shown in Fig. 4.

B. The design of the Camera

The camera unit is assembled using the PCB with 2D PSD and electronic circuitry, C-mount lens and an IR filter. The C-mount lens has a nominal focal length of 35 mm. This lens offers a field of view covering an area of 200 mm x 200 mm at a distance of approximately 800 mm. Focusing quality of the lens does not affect the signal quality in PSDs. The iris of the lens was adjusted to the fully open position to ensure maximum illumination. An IR filter which has a band-pass frequency of 850 nm is used in front of the lens to eliminate noise and background illumination. A serial cable is used to facilitate power and data communication from the camera. An exploded view of the camera is shown in Fig. 5.

The camera will be used to measure the position of an IR marker. In the proposed system it will be mounted on the EE of the robotic arm. A high power IR light emitting diode (LED) from Vishay (VSMY7850X01) is used as the emitting beacon. This is a high intensity LED which illuminates with current flows of up to 1 A. The intensity of the signal will ensure a high signal-to-noise ratio improving the accuracy of the measurement. It is also a wide angle LED which covers

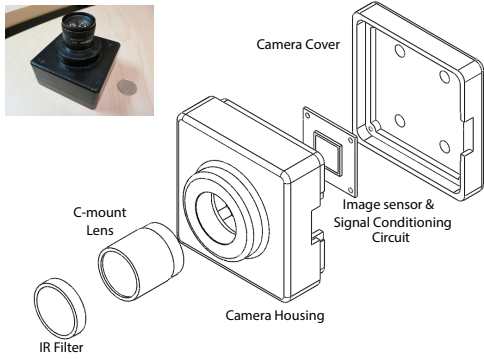


Fig. 5. An exploded view of the PSD camera

a beam angle of 120 degrees allowing the EE to be seen by the camera over a much wider operating envelope.

C. Calibration of the PSD and the Camera Unit

The proposed camera needs to be calibrated before it is used for measuring the position. More emphasis was put on the calibration process since the proposed method uses single sensor feedback for position measurement as compared to Wang et al. [14], who used multiple sensor fusion. The 2D PSD consists of non linearities such as the pin cushion effect. Therefore, it needs to be calibrated to relate the actual position of the IR spot on the sensor with the position obtained from induced currents. For calibrating the 2D PSD, it was mounted onto a precision x-y translation table which is capable of producing displacements in x and y directions with accuracies of up to $10 \mu\text{m}$. An IR illumination source which consists of a laser LED with an aperture size of $100 \mu\text{m}$ was used as the marker for the calibration. The sum of four anode currents indicates the lighting level from the illumination source. A feedback controller was used to maintain the illumination from the marker at a constant level. A set of 10×10 points covering an area $8 \times 8 \text{ mm}$ of the PSD was obtained for analysis.

A Design of Experiments (DOE) based method was used to analyze the data that was obtained through the calibration. The response surface methodology (RSM) is a statistical technique used for developing empirical models from experimental data. In RSM the input variables are known as factors and the output variables are known as responses. The objective of RSM is to optimize a response variable that is influenced by several independent factors. In the given case, responses are the true position of IR spot on the PSD, while factors are x,y positions calculated from the four currents. The calibration data was analyzed using the RSM - IV optimal design method. The best model is determined by considering various statistical parameters such as p value, F value, adjusted and predicted R^2 . In statistics, the p value corresponds to the probability that the null hypothesis is rejected. The F test provide an indicator for comparing the statistical models that would provide a fit to the data set. The best fit model should consist of a lower p value, higher F

value and reasonably close adjusted and predicted R^2 values high in magnitude. The StatEase v8 software was used to analyze the data. The calibration results for the 2D PSD are shown in Fig.s 6,7. The DOE provides the model of best

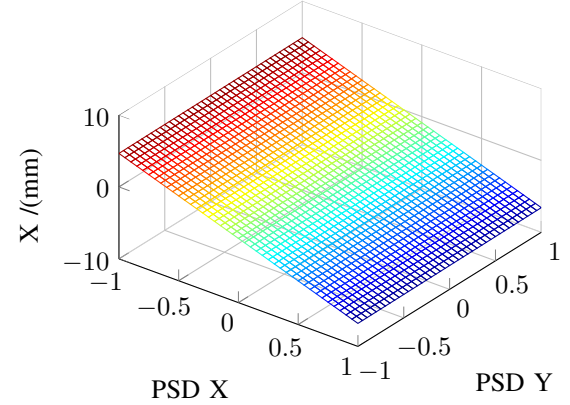


Fig. 6. The variation between X vs $\bar{X}(\text{PSD}X)$ and $\bar{Y}(\text{PSD}Y)$

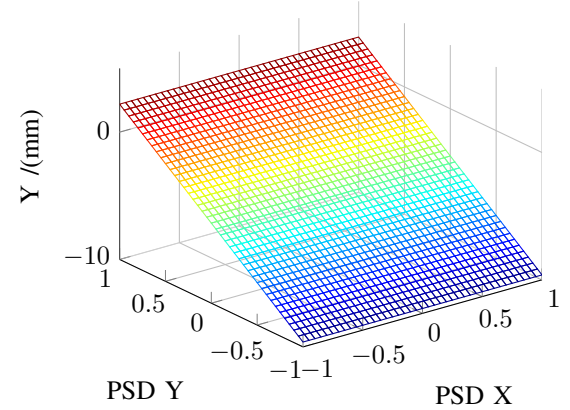


Fig. 7. The variation between Y vs $\bar{X}(\text{PSD}X)$ and $\bar{Y}(\text{PSD}Y)$

fit based on a statistical analysis using the experimental data obtained during the experiments. The models suggested by the analysis are as follows.

$$\text{psd}X = f(k_1, \bar{X}, \bar{X}^2) \quad (4)$$

$$\text{psd}Y = f(k_2, \bar{Y}, \bar{Y}^2, \bar{Y}^3), \quad (5)$$

Where $\text{psd}X$, $\text{psd}Y$ are the true x,y positions of the IR spot on PSD and k_1 , k_2 are constants.

The intrinsic parameters of this camera has been known prior to using it for position estimation. This camera needs to be calibrated to estimate these parameters. An effective calibration process would result in accurate and robust measurement of the position. Several methods have been proposed in literature for camera calibration. Out of them, the methods proposed by Heikkila [17] and Rahman, Krouglisoff [18] were used for calibrating this camera.

Heikkila's method considers a checker board consisting of

an array of circular markers as calibration targets and uses a simplified model for estimating the camera parameters. The calibration target used in this method does not always provide the accuracy expected for a camera calibration process. Since a high degree of precision is required, this camera was mounted onto a camera calibration setup. It consists of an x-y table that uses two ball screws driven by stepper motors. This table could be positioned to an accuracy of $15 \mu\text{m}$. This table also provides backlash compensation improving the accuracy. A high power IR LED was used as marker for calibration. A predefined square grid of 150 mm x 150 mm was considered for marker. The marker was given a translational displacement of 5 mm for each reading. Three parallel planes were considered for data collection. The distance between the planes were 12.7. Each calibration run produced a total of 2700 calibration points.

Once the calibration data was obtained, it was analyzed using the algorithms proposed in Heikkila [17] and Rahman et al. [18]. A summary of results from the calibration is given in Table I. SF corresponds to the scale factor, f

TABLE I
SUMMARY OF THE CALIBRATION RESULTS

Method	Parameter								
	SF	f	u_0	v_0	k_1	k_2	p_1	p_2	ϵ
Heikkila	0.9972	34.70	1.60	-0.92	-2.6	0	5	-5.4	9.2
Rahman	1.0403	35.92	2.87	-0.93	-3.2	0	2	-9.9	8.2

is the focal length, k_1 , k_2 are the coefficients of radial distortions in units of 10^{-3}mm^{-2} and mm^{-4} , p_1 , p_2 are the coefficients of tangential distortions in 10^{-4}mm^{-1} and 10^{-3}mm^{-1} units, and (u_0, v_0) are the coordinates of the modified image center in mm.

Reliability of the calibration depends on the repeatability of the results. The discrepancy between the original calibration data and the reconstructed model is indicative of how well the calibrated model fits the calibration data. This is known as the standard error of the calibration model. The standard deviation of the error of the reconstructed model is higher in Heikkila ($9.2 \mu\text{m}$) compared to Rahman & Krouglcof ($8.2 \mu\text{m}$). Therefore, the estimated camera parameters from the method proposed in Rahman & Krouglcof [18] were selected for developing the camera model. Nevertheless, multiple calibration runs proved that these calibration results are repeatable.

IV. ON SITE CALIBRATION OF THE CAMERA

An on site calibration is required to estimate the extrinsic parameters of the camera. It will provide the parameters required to transform measurements made by the camera to a global fixed coordinate system. In the proposed calibration the EE position is estimated with respect to a global coordinate frame using encoder angles. This is denoted by ${}^w\mathbf{P}$. This could be expressed using homogenous coordinates.

Thus,

$${}^w\mathbf{P} = \begin{bmatrix} l_2.\cos(\theta_2) + l_3.\cos(\frac{\pi}{2} + \theta_2 + \theta_3) \\ l_2.\sin(\theta_2) + l_3.\sin(\frac{\pi}{2} + \theta_2 + \theta_3) \\ 0 \\ 0 \end{bmatrix} \quad (6)$$

The camera provides position measurements with respect to its coordinate system and this is given by ${}^c\mathbf{P}$.

The transformation from the world coordinate frame to camera's coordinate frame could be performed by considering a 4×4 transformation matrix (${}^c\mathbf{T}_w$) and a camera matrix (\mathbf{C}). This is also known as the forward camera model. The estimated position of the EE with respect to the camera (${}^c\hat{\mathbf{P}}$) using the encoder data is given by,

$${}^c\hat{\mathbf{P}} = \mathbf{C} \times {}^c\mathbf{T}_w \times {}^w\mathbf{P} \quad (7)$$

$$\text{Where } \mathbf{C} = \begin{bmatrix} s.f & 0 & u_0 & 0 \\ 0 & f & v_0 & 0 \\ 0 & 0 & 1 & 0 \end{bmatrix} \text{ and } {}^c\mathbf{T}_w = \begin{bmatrix} {}^c\mathbf{R}_w & {}^c\mathbf{t}_w \\ 0 & 1 \end{bmatrix}$$

${}^c\mathbf{R}_w$ is obtained considering successive roll (ψ), pitch (ϕ), yaw (θ) angles about the $-x, -y, -z$ axes and ${}^c\mathbf{t}_w = [t_x, t_y, t_z]^T$ describes the translation between the camera and the world coordinate frame. f is the effective focal length, s is the scale factor or aspect ratio and (u_0, v_0) is the position of the image center.

A cost function is formulated to minimize error between EE position estimated using equation 7 and the actual position measured by the camera. If \mathbf{C} is the total cost, it will be given by,

$$\mathbf{C} = \underset{\forall i}{\operatorname{argmin}} \sqrt{\sum ({}^c\hat{P}_i - {}^cP_i)^2} \quad (8)$$

The Levenberg–Marquardt (LM) algorithm [19] is employed to solve the optimization problem and obtain the parameters which minimizes the given objective function. The parameters estimated by the optimization include the link lengths (l_2, l_3), pose (t_x, t_y, t_z) and orientation (ψ, ϕ, θ) of the camera.

V. FPGA-BASED IMPLEMENTATION OF THE PROPOSED CONTROLLER

The controller was implemented using the Terasic DE0 development board. This development board consists of Altera Cyclone III FPGA. Quadrature decoding and SPI Input for feedback and the SPI output interface for the control signal that drives the servo valve were implemented in hardware. Verilog hardware descriptive language was used to develop the hardware components. A virtual soft processor was implemented in the FPGA to implement functions that are too complex to be implemented in hardware. This processor is optimal for medium-performance applications that do not require a large memory for operations. Programming of this virtual processor is similar to that of a microcontroller or any other processor. Therefore, coding for this processor was carried out in C language. The architecture of proposed single time scale VS system is shown in Figure 8. The proposed embedded system provides a single chip solution for controlling the arm.

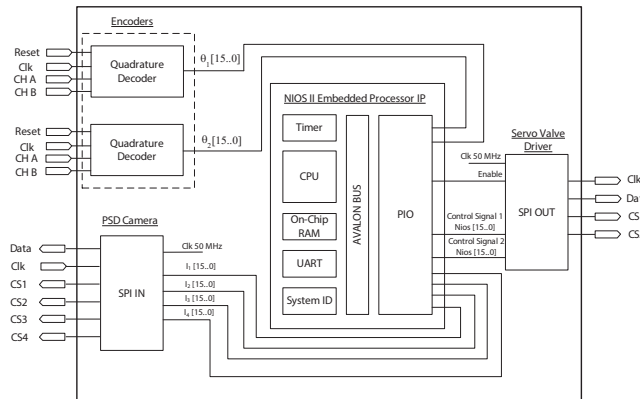


Fig. 8. A schematic diagram showing the architecture of the proposed controller

A NIOS II standard type processor was configured with a 50 MHz phase-locked loop, on-chip memory, a JTAG UART, an interrupt timer and input/output (I/O) ports. The on chip memory comprised 40 kilobytes for running the controller. The JTAG Uart is a universal asynchronous receiver/transmitter which facilitates the data transmission and the communications between the FPGA and a host computer. The interrupt timer was used to trigger a 1 ms interrupt. The input output buses were configured depending on the bit size of the signals.

The robotic manipulator is instrumented with joint encoders to measure the position of joint angles. These encoders have a resolution of 8000 pulses per revolution. The encoders provide the angular position using two pulse trains. The magnitude of joint angle and direction of rotation could be estimated by carrying out quadrature decoding of the two pulse trains. Each encoder requires four flip flops implemented in hardware to perform this operation. The position measurement from the PSD camera is obtained as four digital voltage signals. The ADS8320 ADC requires a 16 bit SPI with data in protocol. The electronic design of the circuit used a common data and clock input with four different chip selects for data acquisition. The SPI input protocol was implemented in hardware. The data acquisition from the ADC could be carried out at data rates of up to 12 kHz. In order to eliminate noise from the voltage signals of the PSD a soft-coded median filter was used.

The control signal was calculated in the soft processor using the feedback signals. This signal will be output to a DAC via 16-bit SPI output interface. It consists of a clock, data and a chip select signal. This interface was developed in hardware so that it is compatible with the timing diagram of the MAX541 DAC converter. The analog voltage from the DAC is sent to the servo valves via an operational amplifier circuit which amplifies the signal.

VI. THE EXPERIMENTAL SETUP

The SCARA manipulator considered in study has two links and an EE. The links of this manipulator are 0.49m

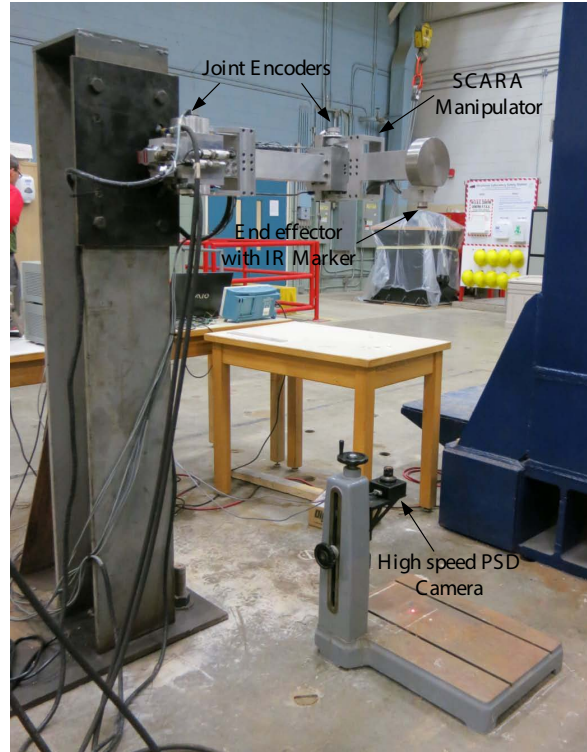


Fig. 9. Experimental setup with the SCARA manipulator

and 0.36m in length. Double vane rotary hydraulic actuators with integrated hydraulic servo valves are used to drive the revolute joints of this manipulator. These actuators operate at a rated hydraulic system pressure of 3000 psi. The second link incorporates an EE which has a weight of 12 kg. This SCARA Arm is mounted onto a compliant support with an 'I' shaped cross section. The joints of this robot are instrumented with rotary encoders as proprioceptive sensors.

The high speed camera developed in this study is used as the exteroceptive sensor. It will be mounted opposite to the EE of the manipulator. The high power IR LED is mounted on to the EE of the arm. The camera will provide the position of the EE. The proposed high speed visual servoing system is shown in Fig. 9.

VII. EXPERIMENTAL RESULTS

A. Accuracy of the High Speed Camera System

The on-site calibration algorithm was presented in section IV. It uses an iterative scheme with LM method to optimize a cost function to provide the on-site parameters which include position and orientation of the camera. A data set was obtained by moving the EE over a 10 x 10 mm grid. The data set obtained include the encoder readings and four voltages from the camera. The position provided by the joint encoders is considered as the true position. The voltage signals provided by the camera are median filtered and converted into position signals taking into account the non linearities of the image sensor.

Fig. 10 (a) show a plot of the root mean squared error (RMSE) between the measurements in $-x$ and $-y$ directions

before calibration. An accurate measurement would result in points that are concentrated around $(0, 0)$. However, it is seen that these points are mainly concentrated in 2nd and 3rd quadrants. This offset indicates that the position of the image center has to be re-estimated. The Fig. 10 (b),(c) show plots of the absolute value of the RMSE in x,y directions. It is seen that the error follows a fairly repetitive pattern as the accuracy of the position measurements decrease with the distance from image center. It is also seen that the error in measurements in $-x$ direction is higher compared to that in $-y$ direction.

The results obtained after the calibration is shown in Fig 11. It could be seen that the measurement error has rapidly decreased after the on-site calibration. If the extrinsic parameters are not considered the absolute error could be as high as 3.7 mm in x - direction and 2.34 mm in y -direction, respectively. The absolute average RMSE in x -direction will decrease from 1.43 mm to 0.31 mm and in y -direction it will decrease from 0.73 mm to 0.37 mm. Once the on-site calibration carried out the absolute RMSE will not exceed 1 mm in both x, y directions. For the calibration points considered the maximum absolute error was 0.93 mm in x - direction and 0.95 mm in y - direction, respectively. The on-site calibration produces a significant improvement in the accuracy of the measurement.

The Fig. 10, 11(d) shows the absolute value of the cost function for each data point. This represents an error in a distance measurement from the origin of the Cartesian coordinate frame. The cost function has an average RMSE of 1.71 mm before the calibration. The RMSE of the cost function could be as high as 3.71 mm at times. However, with the calibration the the average RMSE will reduce to 0.54 mm. Therefore, once calibrated this camera is robust in performance to carry out position measurements. The experiments show that in $-x$ direction this camera is capable of providing measurements with an average accuracy of 0.31 mm with a standard deviation of 0.26 mm. In $-y$ direction the average accuracy was 0.37 mm with a standard deviation of 0.24 mm.

B. Testing of the Proposed VS system

The SCARA arm considered in this study is capable of reaching very high velocities. Since the EE carries a considerable payload it results in significant deflection in the support column. Therefore, the absolute position of the EE needs to be obtained and to be used in controlling the arm. The EE was set to follow a desired linear trajectory on the work profile from (425 mm, 333 mm) to (550 mm, 232 mm). The trajectory following experiment considered two different cases. In one of the cases it considered only the encoder feedback (with no VS). Thus, effects of the external disturbances were not considered in the control algorithm. In the other case with VS, it considered feedback from the encoders and the camera.

Experiments showed that the camera developed in this study was capable of providing position measurements of up to 1340 Hz. The experimental results showing the desired

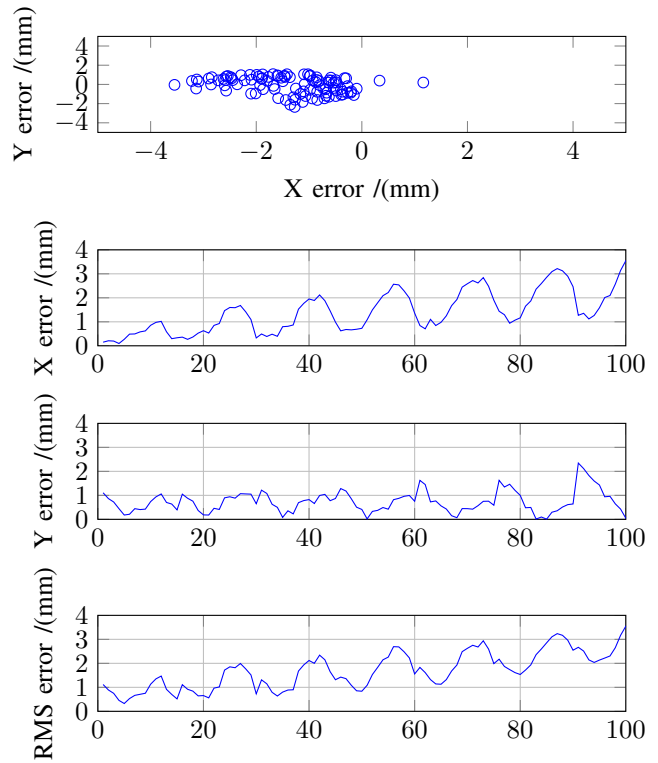


Fig. 10. The error of the camera before calibration

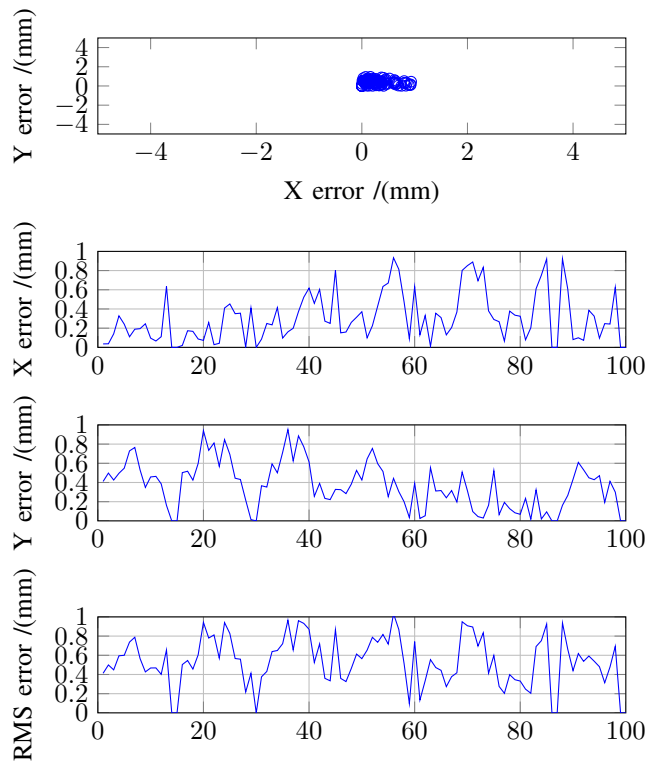


Fig. 11. The error of the camera after calibration

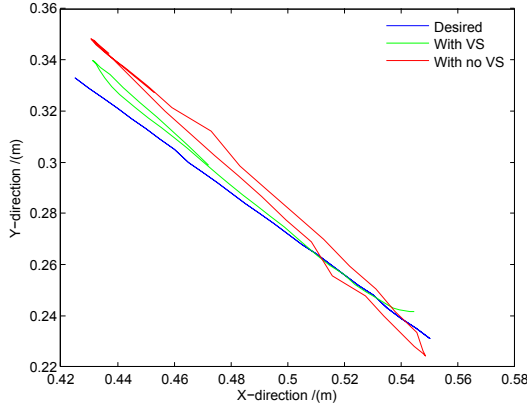


Fig. 12. EE following a given trajectory with and without VS

path of the EE and the actual path which EE traced is shown in Fig. 12. It is seen from the experimental results that, VS improved the accuracy of the trajectory that was followed by the EE. Nevertheless the feedback from the camera and encoders were considered simultaneously in this single time scale VS system. During the experiments the average EE velocity was 1.3 ms^{-1} . The control signal was updated at a frequency of 330 Hz.

VIII. CONCLUSIONS

In this study, we have proposed a method to perform single time scale VS. It outlined the development of a high speed camera system for position measurement. This camera uses a 2D PSD as the image sensor. The electronic circuitry for performing signal conditioning and data acquisition was developed. Then the 2D PSD was calibrated to relate the actual position of the IR spot on the sensor to the position obtained from induced voltages. Next the camera was assembled to a housing along with the printed circuit board with the PSD, a C-mount lens with a nominal focal length of 35 mm and an IR filter. This camera was mounted on to a camera calibration setup to estimate the intrinsic parameters of the camera. A methodology for on site calibration was developed for estimating the position and orientation of the camera once is mounted to the application setup. An FPGA based embedded system was developed for implementing the controller. It used both hardware and a soft processor for feedback and executing the control algorithm.

This camera was capable of providing measurements at frequencies of up to 1340 Hz. The position measurements provided by the camera was accurate up to 0.93 mm, 0.95 mm in x -, y - directions, respectively. The proposed single time scale VS system was experimented with a high speed SCARA type manipulator with servo hydraulic actuators. The experimental results showed a satisfactory performance of the proposed VS system at EE speeds of up to 1.3 ms^{-1} . The VS controller operated at a frequency of 330 Hz during the experiment.

REFERENCES

- [1] L. Bascetta and P. Rocco, "Two-time scale visual servoing of eye-in-hand flexible manipulators," *Robotics, IEEE Transactions on*, vol. 22, no. 4, pp. 818–830, 2006.
- [2] Z.-H. Jiang and T. Eguchi, "Vision feedback based end-effector motion control of a flexible robot arm," in *Systems, Man and Cybernetics, 2007. ISIC. IEEE International Conference on*, oct. 2007, pp. 2413 –2419.
- [3] Y. Liu, N. Xi, Y. Shen, S. Bi, B. Gao, Q. Shi, X. Li, G. Zhang, and T. Fuhlbregge, "High-accuracy visual/psd hybrid servoing of robotic manipulator," in *Advanced Intelligent Mechatronics, 2008. AIM 2008. IEEE/ASME International Conference on*, 2008, pp. 217–222.
- [4] G. Hitaka, T. Murakami, and K. Ohnishi, "An approach to vibration control by stereo vision system in mobile manipulator," in *Advanced Intelligent Mechatronics, 2001. Proceedings. 2001 IEEE/ASME International Conference on*, vol. 1, 2001, pp. 601 –605 vol.1.
- [5] W. Song and M. Minami, "Hand to eye vergence dual visual servoing to enhance observability and stability," in *Robotics and Automation, 2009. ICRA '09. IEEE International Conference on*, 2009, pp. 714–721.
- [6] R. Kelly, "Robust asymptotically stable visual servoing of planar robots," *Robotics and Automation, IEEE Transactions on*, vol. 12, no. 5, pp. 759–766, 1996.
- [7] M. Marey and F. Chaumette, "Analysis of classical and new visual servoing control laws," in *Robotics and Automation, 2008. ICRA 2008. IEEE International Conference on*, 2008, pp. 3244–3249.
- [8] T. Sievers and S. Fatikow, "Visual servoing of a mobile microrobot inside a scanning electron microscope," in *Intelligent Robots and Systems, 2005. (IROS 2005). 2005 IEEE/RSJ International Conference on*, aug. 2005, pp. 1350 – 1354.
- [9] P. Rousseau, A. Desrochers, and N. Kruglicof, "Machine vision system for the automatic identification of robot kinematic parameters," *Robotics and Automation, IEEE Transactions on*, vol. 17, no. 6, pp. 972 –978, dec 2001.
- [10] J. Fischer and O. Pribula, "Precise subpixel position measurement with linear interpolation of cmos sensor image data," in *Intelligent Data Acquisition and Advanced Computing Systems (IDAACS), 2011 IEEE 6th International Conference on*, vol. 1, sept. 2011, pp. 500 –504.
- [11] A. Tobergte, F. Frohlich, M. Pomarlan, and G. Hirzinger, "Towards accurate motion compensation in surgical robotics," in *Robotics and Automation (ICRA), 2010 IEEE International Conference on*, may 2010, pp. 4566 –4572.
- [12] N. Michael, D. Mellinger, Q. Lindsey, and V. Kumar, "The grasp multiple micro-uav testbed," *Robotics Automation Magazine, IEEE*, vol. 17, no. 3, pp. 56 –65, sept 2010.
- [13] M. Windolf, N. Götzén, M. Morlock *et al.*, "Systematic accuracy and precision analysis of video motion capturing systems—exemplified on the vicon-460 system." *Journal of biomechanics*, vol. 41, no. 12, p. 2776, 2008.
- [14] C. Wang, W. Chen, and M. Tomizuka, "Robot end-effector sensing with position sensitive detector and inertial sensors," in *Robotics and Automation (ICRA), 2012 IEEE International Conference on*, may 2012, pp. 5252 –5257.
- [15] M. Liyanage, N. Kruglicof, and R. Gosine, "Development and testing of a novel high speed scara type manipulator for robotic applications," in *Robotics and Automation (ICRA), 2011 IEEE International Conference on*, may 2011, pp. 3236 –3242.
- [16] "Hamamatsu s5991 data sheet," Hamamatsu Photonics K.K., Hamamatsu, Japan.
- [17] J. Heikkila, "Geometric camera calibration using circular control points," *Pattern Analysis and Machine Intelligence, IEEE Transactions on*, vol. 22, no. 10, pp. 1066 – 1077, oct 2000.
- [18] T. Rahman and N. Kruglicof, "An efficient camera calibration technique offering robustness and accuracy over a wide range of lens distortion," *Image Processing, IEEE Transactions on*, vol. 21, no. 2, pp. 626 –637, feb. 2012.
- [19] K. Levenberg, "A method for the solution of certain non-linear problems in least squares," *Quarterly of Applied Mathematics*, vol. 2, no. 2, p. 164168, 1944.